Appl. Phys. A 44, 123–130 (1987)

Applied Physics A Solids and Surfaces

Photopyroelectric Spectroscopy (P^2ES) of Electronic Defect Centers in Crystalline n-CdS

A. Mandelis, W. Lo, and R. E. Wagner

Photoacoustic and Photothermal Sciences Laboratory,
Department of Mechanical Engineering, University of Toronto,
Toronto, M5S 1A4, Canada

Received 14 March 1987/Accepted 29 May 1987

Abstract. Photopyroelectric spectroscopy (P^2ES) of n-CdS single crystals was performed at an open circuit, and in conjunction with photocurrent spectroscopy (PCS) in the presence of an applied ac or dc transverse field. The results showed that P^2ES is very sensitive to the presence of deliberately introduced subbandgap defect structures, with the P^2E signal dominated by non-radiative de-excitation mechanisms at defect centers. The potential of this technique as a powerful electronic defect diagnostic tool, combined with the overall experimental simplicity, was demonstrated with mm-thick crystals used as received in an open-cell geometry.

PACS: 72.20, 61.70

There exists a continuous need for nearly perfect II–VI compound semiconductors for use in microelectronic and optoelectronic device technologies. Such materials have the tendency, however, to form intrinsic defects and to deviate from stoichiometry, depending on the preparation method [1]. Pure and specially doped CdS single crystals are finding increasing applications as photoconductive, photovoltaic and optoelectronic devices. Further recent applications of pure CdS as the active element in solid state excitonic lasers at low temperatures [2] have accentuated the demand for defect and impurity-free samples of this semiconductor for high optical gain performance. It is, however, crucial to develop spectroscopic techniques with high sensitivity to the presence of the complex electronic defect networks in CdS and other compound semiconductors, with a view to identify the contributions of such defect centers to undesirable non-radiative energy emission and ultimately associate this behavior with specific phases of the crystal growth or device fabrication process. In the past few years photoacoustic spectroscopy (PAS) has proven to be a particularly sensitive technique in monitoring non-radiative defect centers in CdS both in the piezoelectric detection mode [3] and the microphonic mode at room [4] and at cyrogenic [5] temperatures. Siu and Mandelis gave a theoretical interpretation of the PA spectra from n-CdS in terms of their dependence on the wavelength-dependent non-radiative quantum efficiency in the defect-rich subbandgap region [6] in the presence of other competing de-excitation channels, such as photocurrent generation upon application of external electric fields, or radiative transitions (luminescence). The validity of that theory was further corroborated by experimental agreement with photocurrent (PC) spectra. A comprehensive review of CdS PAS was recently presented by Mandelis [7], and definitions pertinent to non-radiative phenomena in CdS have been given by Mandelis and Siu [4].

The important low temperature region, however, still remains somewhat problematic, if the use of microphone gas-coupled PAS is opted for, due to acoustic noise associated with the separation of sample and microphone chambers and the presence of liquid nitrogen [4]. Acoustic noise is also inevitably present at room temperature as well as in piezoelectric detec-

tion contributing to the relatively low signal-to-noise ratio (SNR).

Photopyroelectric spectroscopy (P^2ES) has recently emerged as a simple, powerful photothermal technique for the spectroscopic study of condensed phase materials [8–13]. Pyroelectric thin-film sensors, such as polyvinylidene difluoride (PVDF) [14] have proven to be capable of providing high SNR, high quality spectra of thin-film materials [8, 11, 15], as well as spectra of condensed phase samples in the thickness range above 200 μm [10].

In this work we exploited the non-acoustic nature of the detection mechanism of thin-film P^2ES to obtain high quality, high SNR spectra of n-CdS single crystals pyroelectrically for the first time. The back-detection character of P^2ES proved to yield extreme sensitivity to subbandgap defect centers, superior to microphonic PAS. The overall simplicity and open-cell geometry of the detection method further point to P^2ES as an optimum photothermal spectroscopy for non-radiative defect studies in semiconductors.

1. Materials and Experimental

CdS samples used in this work were high purity n-type single crystals from Eagle-Pitcher, Inc., Miami, Oklahoma with nominal resistivity $\varrho = 1.3 - 1.9 \times 10^5\ \Omega$-cm. The nominal mobilities were 190–215 $cm^2\ V^{-1}\ s^{-1}$. The crystal growth details were published elsewhere [4]. The crystals were cut with the optic c-axis parallel to the surface plane. They were etched in 95% by volume of 3M HCl and 5% by volume of 30% H_2O_2 in H_2O to remove any surface damage which might distort the photopyroelectric (P^2E) spectra at and below the bandgap energy E_g [16]. Electrical connections were made using an In-Ga mixture at opposite crystal edges with surface normals perpendicular to the detection of incident radiation. This metal-semiconductor interface was shown to exhibit approximately ohmic characteristics in the voltage range between −10 V and + 20 V, with a slight change in the slope of the I–V curve upon reversal of the sign of the field [4].

The experimental system used for combined photopyroelectric and photoconductive spectroscopic studies is shown in Fig. 1. The CdS samples were electrically isolated from the PVDF Ni–Al metallization by a thin Teflon membrane stretched over the polyelectric film which was housed in an Inficon™ quartz microbalance sputtering sensor body assembly (Model 007-048) with a crystal holder (Model 007-049) and a ceramic retainer (Model 007-023). This assembly, conventionally used as a quartz crystal housing, was readily adapted to mount PVDF thin-films, offering mechanical support, rf shielding and electrical contacts. The Teflon membrane, besides electrically decoupling the samples from the detector, served as a barrier to direct PVDF film irradiation at subbandgap wavelengths where CdS is optically transparent. The mounting of PVDF thin film detectors in the rf shielded housing was accomplished using the method described by Coufal and Peterson [17]. The optical circuit shown in Fig. 1 used randomly polarized light from a 1000 Xe lamp (Oriel Model 6141) to photoexcite CdS crystals simply held in position on top of the Teflon membrane with a mechanical screw assembly applying gentle pressure and ensuring intimate thermal contact with the detector. ac voltages were applied to CdS using a Krohn-Hite model 5100 A generator. dc voltages were applied using a Coutant model LQ 100/30 voltage/current generator. All P^2E amplitude spectra were normalized by the Xe lamp spectrum obtained using the bare PVDF film covered with the Teflon membrane as the detector, and stored in the computer memory for later use. Similarly, all P^2E phase spectra used in this work are the result of

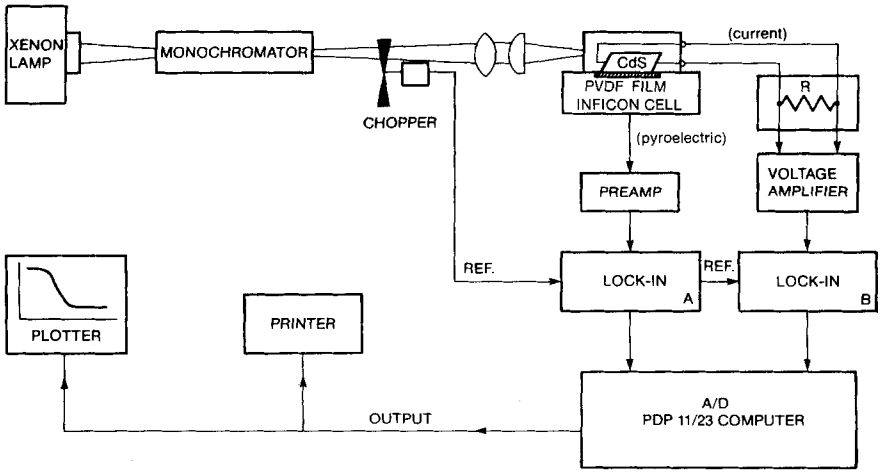

Fig. 1. Schematic diagram of the experimental apparatus for P^2ES and PCS measurements

subtraction of the Teflon-covered detector phase spectrum.

2. Results and Discussion

Three kinds of experiments were performed at room temperature: (a) open-circuit P^2ES; (b) P^2ES and PCS with an applied transverse dc bias; and (c) P^2ES and PCS with an applied transverse ac bias.

2.1. Open-Circuit P^2E Spectra

The open-circuit P^2E absorption spectrum of a CdS crystal is shown in Fig. 2. At the modulation frequency f of the experiment (3 Hz) the thermal diffusion length μ_s in CdS is

$$\mu_s(f)=(\alpha_s/\pi f)^{1/2} \tag{1}$$

or, $\mu_s(3\,\text{Hz})=1.26$ mm, using [18] the value for the thermal diffusivity of CdS $\alpha_{CdS}=0.15$ cm^2/s. Therefore, the 1 mm thick sample is essentially thermally thin at 3 Hz and the P^2E signal is proportional to the absorptance and hence to the optical absorption coefficient of CdS [12] under conditions of constant thickness. The position of E_g at ca. 500 nm in Fig. 2 is in agreement with transmission measurements of that quantity reported elsewhere [4]. In what follows λ_g will be defined to be the wavelength associated with the band-gap energy.

Previous photopyroelectric spectroscopic measurements [9, 11] indicate, and the developed theory [12] predicts, that there occurs an inversion in the spectral character of P^2E spectra with increasing modulation frequency above a transition frequency f_0 such that

$$\mu_s(f_0)\approx L, \tag{2}$$

where L is the sample thickness. As the material becomes thermally thick, the absorption spectrum gradually becomes a transmission spectrum. For our CdS single crystal of Fig. 2, $f_0\approx 5$ Hz. Figure 3a shows the onset of spectral inversion at ca. $f=6$ Hz (ampli-

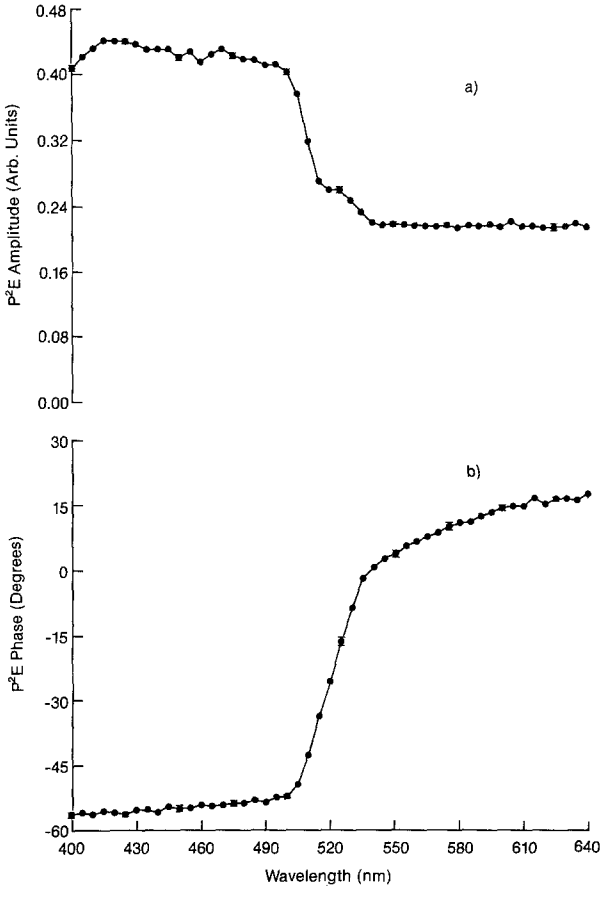

Fig. 2a and b. Normalized photopyroelectric spectrum of n-CdS single crystal in the band-gap region. Thickness: 1 mm; modulation frequency: 3 Hz; (a) Amplitude, (b) Phase (Resolution: 2 nm)

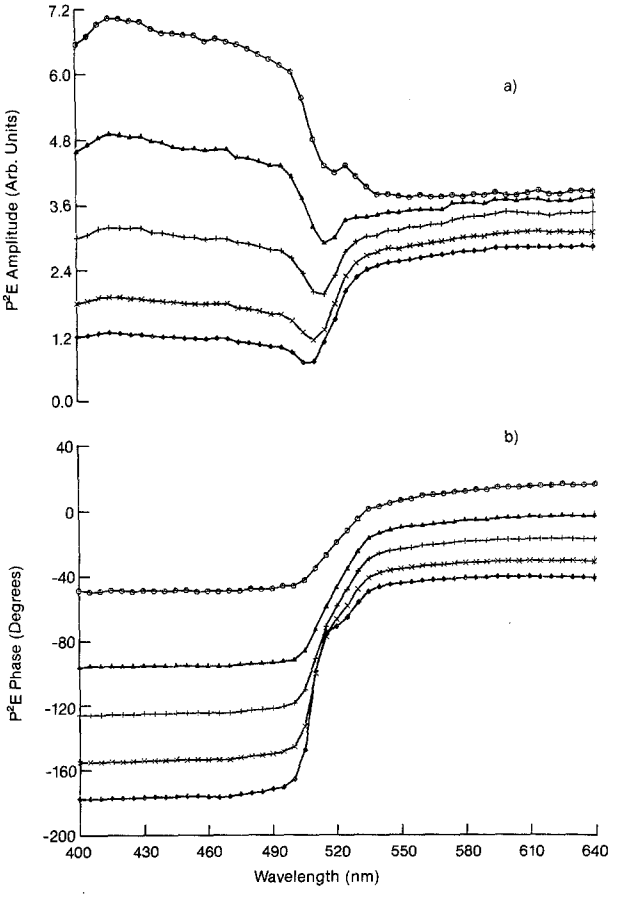

Fig. 3a and b. Modulation-frequency dependence of photopyroelectric spectra of CdS crystal (1 mm thickness) –O–O–: 3 Hz; –△–△–: 6 Hz; +–+–: 9 Hz; ×–×–: 12 Hz; ◆–◆–: 15 Hz; (a) Amplitude, (b) Phase (Resolution: 2 nm)

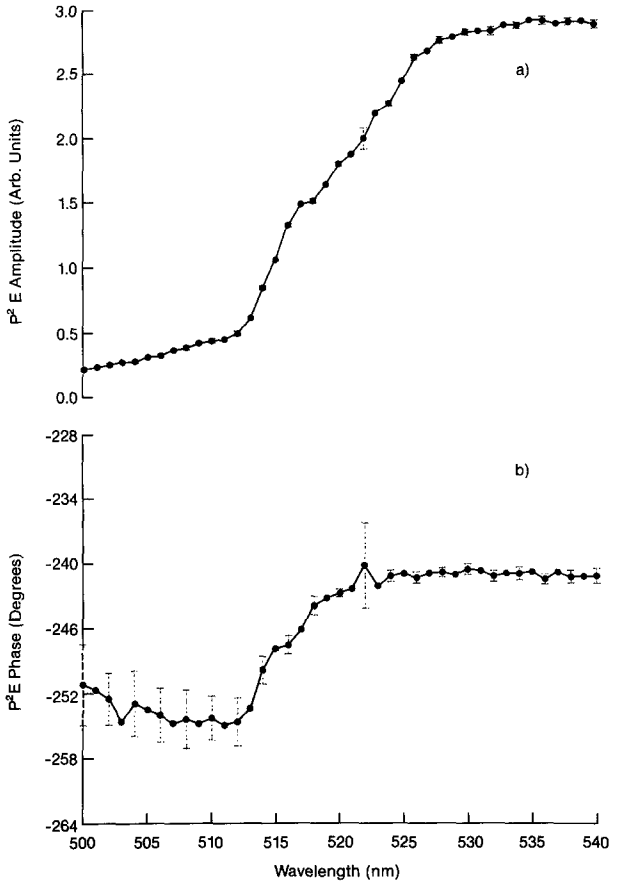

Fig. 4a and b. Photopyroelectric spectrum of n-CdS single crystal with narrowline fracture. Thickness ca. 0.4 mm; modulation frequency: 2 Hz; (a) Amplitude, (b) Phase (Resolution: 2 nm)

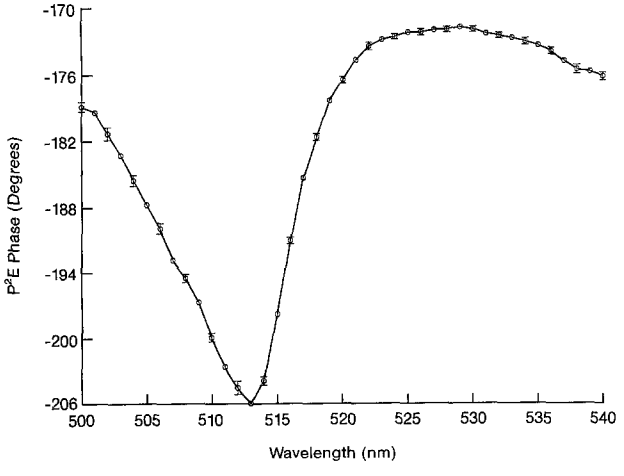

Fig. 5. P^2ES phase of n-CdS single crystal with narrowline fracture. Thickness ca. 0.4 mm; modulation frequency: 75 Hz (Resolution: 2 nm)

tude spectrum). The P^2E phase, however, does *not* exhibit inversion characteristics (Fig. 3b) in agreement with the photopyroelectric theory [12]. Although thin PVDF films are known to exhibit piezoelectric behavior and have been used to measure acoustic vibrations by means of pulsed laser excitation [19], the observed qualitative agreement of the spectral inversions in Fig. 3 with the purely photopyroelectric theory of [12] was a good indicator that we were only observing pyroelectric effects in our experiments. This was further corroborated with negligible acoustic ringing of the mounted PVDF films.

A thin n-CdS crystal exhibiting the low frequency spectrum of Fig. 2 was further etched to thickness ca. 0.4 mm, so that the condition

$$\mu_s(2\,\text{Hz}) = 1.55\,\text{mm} \gg L \tag{3}$$

was valid and the sample was definitely thermally thin. When deliberate mechanical damage was introduced to the crystal in the form of a narrowline fracture along the *c*-axis which did not entirely sever the crystal, but introduced a damage network below the surface and outward from the fracture line, the 2 Hz P^2E spectrum of the crystal exhibited strong inversion of features with respect to the curves of Fig. 2a, with the subbandgap signal increasing approx. tenfold over its value before the fracture (Fig. 4a) while the superbandgap signal remained essentially unchanged (compare with Fig. 2a). The P^2E phase of the intact crystal (Fig. 2b) shows a gradual increase (indicated as a more positive value in this and later figures, and henceforth designated as a "phase lead"; the opposite effect will be designated as a "phase lag") over ca. 100 mm span before saturating in the region above λ_g, as expected from the shift of the heat centroid from the remote front crystal surface (opaque superbandgap region; $\lambda < 490$ mm) into the bulk and closer to the back PVDF detector with decreasing optical absorption coefficient. This trend has been interpreted theoretically previously [12]. The P^2E phase of the fractured crystal, however, (Fig. 4b) is characterized by a much more abrupt increase above λ_g of ca. 10 nm span before saturation. Below λ_g, the phase exhibits a minimum at ca. 513 nm (which corresponds to a maximum in phase lag) in lieu of the monotonic behavior shown in Fig. 2b. This phase minimum becomes more pronounced with increasing modulation frequency as was verified with experiments performed at 6, 10, and 75 Hz. The P^2E phase at 75 Hz is shown in Fig. 5, which shows that the spectral position of the maximum lag remained unchanged with frequency at ca. 513 nm. A spectral behavior similar to that of Fig. 2b of the phase of an intact CdS single crystal in a microphone gas-coupled PA cell with back surface detection has been observed by Takaue et al. [20] at frequencies ranging from 8 to 80 Hz, with a flat superbandgap profile and a broad subbandgap increases with onset around 520 nm and a span of ca. 100–120 nm before saturation. The frequency-dependent P^2E phase increase below 513 nm in Figs. 4b and 5 is most likely related to the

perturbed heat centroid location after the introduction of damage. In the presence of large densities of non-radiative defects the heat centroid may no longer be dominated entirely by the optical absorption length in the material, but rather by bulk defect centers via their contributions to the wavelength dependent non-radiative quantum efficiency, $\eta_{NR}(\lambda)$. In this case, the observed phase increase below 513 nm in Fig. 5 would be explained by the domination of defect densities in proximity to the front crystal surface, where such densities are expected to be the highest in the vicinity of the fracture line in spectral regions near E_g where $\beta(\lambda)L \approx 1$ [$\beta(\lambda)$: optical absorption coefficient]. Consequently, the spectral characteristics of the P^2E signal vs. wavelength would depend on $\mu_s(f)$ and would change as a function of modulation frequency as observed in Figs. 4b and 5. On the other hand, the more abrupt change in phase at $\lambda > 513$ nm registered in Figs. 4b and 5 than that in Fig. 2b may be due to the difference in sample thickness (0.4 mm vs. 1 mm, respectively): As the wavelength is scanned from below to above the band-gap, the heat centroid in the thinner sample should traverse a shorter distance over a smaller λ range than in the thicker sample, thus exhibiting a more abrupt phase change [21]. These proposed mechanisms are in qualitative agreement with the phase spectra of Figs. 4b and 5 and intermediate ones obtained at 6 and 10 Hz.

2.2. P^2E and PC Spectra: Modulated Optical Excitation with dc Electric Field

To test further some of these ideas several experiments were performed with a dc voltage applied transversely across the CdS crystal. The magnitude of the applied bias was varied between 5 and 30 V. Both photopyroelectric and photocurrent spectra from the fractured crystal were obtained simultaneously and are shown in Figs. 6 and 7. In Fig. 6a the spectrum corresponding to the $V_{dc} = 0$ V case, when expanded, is described by that of Fig. 4a for the fractured crystal. The P^2E and PC amplitudes (Figs. 6a and 7) respectively, show large increases with increased bias and a maximum at ca. 529 nm, in agreement with previous photoacoustic data [4, 5]. No local maximum at shorter wavelengths can be identified in the P^2E spectrum, unlike the PA spectra of crystals from the same batch reported in [5]. We attribute the absence of the high energy peak to complete spectral domination by the large increase of the sub-band-gap P^2E signal due to the enhanced Joule effect [4, 5, 22] in the presence of non-radiative scattering centers, perhaps in conjunction with the suppression of interband transition features due to the back surface detection, as observed previously by Hata et al. [23] with a

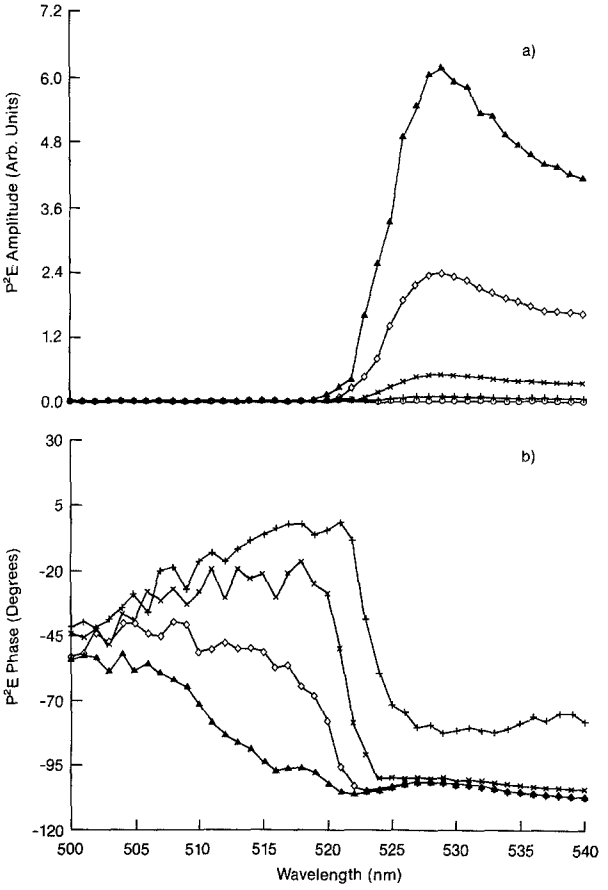

Fig. 6a and b. P^2E spectra of n-CdS single crystal (narrowline fracture) with an applied transverse dc bias of 0 V (–○–○–); 5 V (+–+–); 10 V (×–×–); 20 V (◆–◆–); 30 V (▲–▲–); (a) Amplitude, (b) Phase. $f = 10$ Hz (Resolution: 2 nm)

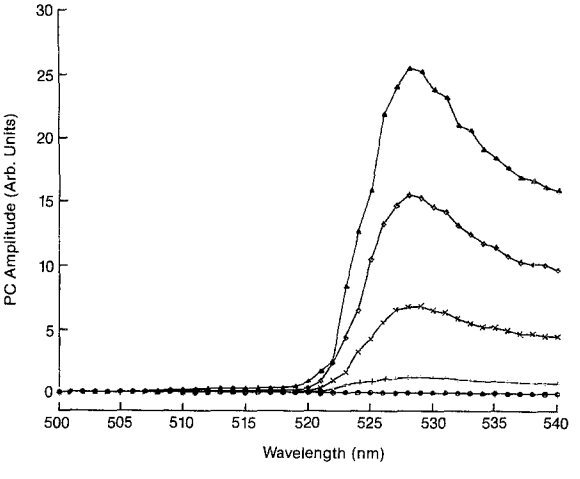

Fig. 7. PC spectra corresponding to Fig. 6

piezoelectric transducer. The P^2E and PC amplitude decay to very small values below λ_g in Figs. 6a and 7 is consistent with surface excitation and the absence of bulk carrier contributions to either signal, in agreement with earlier observations [4, 5, 21, 22]. The strong

peaks in the P^2E spectra of Fig. 6a and PC spectra of Fig. 7 were identified photoacoustically [6] to be consistent with the spectral variation of the non-radiative quantum efficiency $\eta_{NR}(\lambda)$ in the presence of large defect densities. The PC phases for all applied biases essentially coincided below λ_g and exhibited a slight downward trend (lag) at long wavelengths similar to that reported in [5]. The P^2E phase spectra of Fig. 6b show suppresion of the sub-band-gap lead exhibited for $V_{dc}=0$ V in Figs. 4b and 5. The observed lag saturates for $V_{dc}>10$ V at long wavelengths and is consistent with increasing domination of the sub-band-gap signal by the electric field-induced, spatially integrated Joule heating [4]. It can be concluded from Fig. 6b that the heat centroid in the defect-rich crystal, when dominated by the Joule effect, lies closer to the front surface than that due to defect center non-radiative release at $V_{dc}=0$ V, assuming that the increased phase lag with increasing V_{dc} is the result of the bulk heat centroid moving closer to the front surface in this back detection experiment, as argued earlier in discussing Figs. 4b and 5. For higher values of the dc electric field, Joule phenomena are expected to dominate larger spectral ranges up to photon energies close to E_g, where surface absorption becomes predominant and the P^2E phase spectra become independent of the value of the field. These trends can be seen as blue shifts of the phase spectra with increasing V_{dc} in Fig. 6b, as well as "bunching" of all spectra at $\lambda=500$ nm for all values of V_{dc}. The actual phase behavior with V_{dc} in the wavelength range between 500 and 525 nm is expected to be a complicated function of electron-defect interaction in the crystal, its optical spectrum and the modulation frequency of the thermal probe. On the other hand, lock-in detected PC spectra are a measure of the peak values of free carrier density generation rates per wavelength with amplitude decreasing with increasing modulation frequency, since the total number of photogenated carriers per period decreases. This trend was verified in our previous combined PA/PC study of n-CdS [4] and was also observed in the present work. The PC phase, however, does not depend on thermal diffusion mechanisms, but rather on electronic transport which is very fast compared with the range 2–75 Hz used in these experiments. It is thus expected to be independent of modulation frequency *and* of the actual value of V_{dc}, in agreement with our observations.

2.3. P^2E and PC Spectra: Unmodulated Optical Excitation with ac Electric Field

The main difference between this mode of experimentation and the preceding one is that this mode is *only* sensitive to thermal energy released due to the Joule effect in the crystal (P^2E spectra), while PC spectra are dominated by electronic transport of carriers which survive Joule effect scattering and decay. This is so, because the photogenerated carrier densities are dc (unmodulated), and therefore thermal energy from non-radiative carrier recombination is also not temporally modulated and thus will not be lock-in detected by the P^2E and PC probes. The only ac dependence in the sample is that due to the alternating electric field $E(t)$ contributing a Joule heat density proportional to $E^2(t)$ and to the dc photogenerated carrier density [5, 6, 22]. Therefore, a simpler interpretation of the experimental responses than that of Sect. 2.2 is expected with this mode of experimentation. The magnitudes and phases of the P^2E and PC spectra with a 20-V peak-to-peak ac electric field applied transversely across the defect-rich CdS crystal are shown in Figs. 8 and 9. The P^2E maximum, in Fig. 8a occurs at 529 nm for all modulation frequencies, i.e. in the same spectral location as the maxima in Fig. 6a; so do the PC maxima in Fig. 9a, similar to those in Fig. 7.

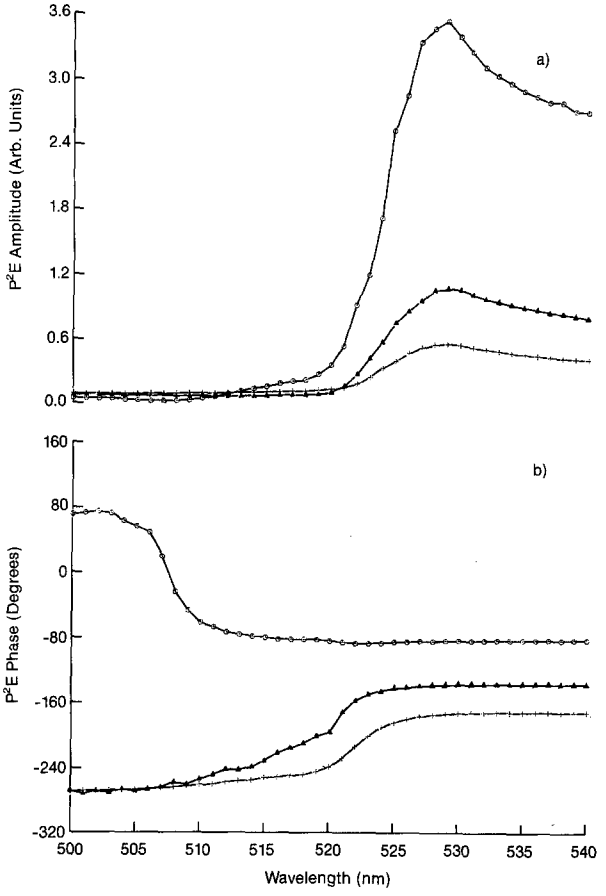

Fig. 8a and b. Magnitude (a) and Phase (b) spectra of P^2E responses from defect-rich CdS crystal with an ac transverse electric field of 20 V peak-to-peak. (–o–o–): 20 Hz; (–▲–▲–): 40 Hz; (–+–+–): 55 Hz (Resolution: 2 nm)

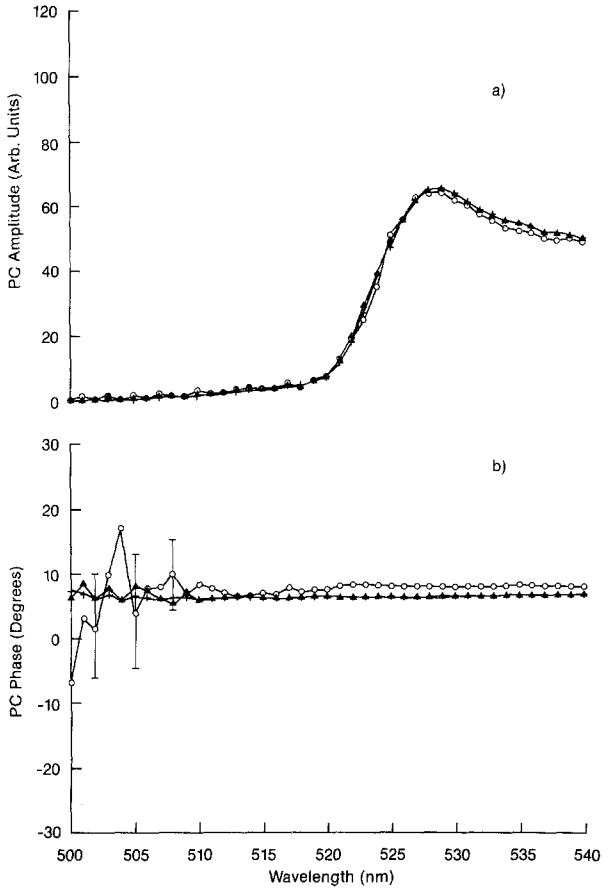

Fig. 9. (a) and (b) PC spectra corresponding to Fig. 8

The constancy of the spectral position of the P^2E 528–529 nm maximum with mode of experimentation (dc or ac electric field applied) and under different modulation frequencies was previously observed photoacoustically [4] and interpreted as related to the wavelength-dependent non-radiative quantum efficiency. The independence of the PC magnitude (Fig. 9a) from modulation frequency is also expected, as the free carrier density within the crystal (the quantity directly related to be PC magnitude) is not affected by the low modulation frequencies employed here, compared to the carrier response rate. The P^2E magnitude response is, of course, thermal diffusion-limited and exhibits large attenuation with increasing frequency (Fig. 8a).

Under unmodulated optical excitation and photocarrier orientation in the presence of the external ac electric field, the generation and recombination of free carriers are dc phenomena and thus carrier lifetimes should not affect the thermal wave (P^2E) phase response [4, 24]. The increase in the P^2E phase lag ($f=20$ Hz) observed in Fig. 8b can be attributed to sub-band-gap domination by bulk Joule heating, consistently with the behavior exhibited in Fig. 6b. The phase inversions observed in Fig. 8b for $f>20$ Hz are not well understood at this time, however, the effective phase lead which appears at $\lambda \geqq 515$ nm could be indicative of the domination of the thermal wave signal by non-radiative defect energy release deep in the bulk (i.e., closer to the detector), over the smaller, (and closer to the front surface) volume probed by the shorter thermal diffusion length-limited Joule effect at higher frequencies. This conjecture would be consistent with the well-known fact that back-detection thermal wave techniques carry information integrated over the *entire* body of the sample, unlike microphone gas-coupled PAS, which detects a temperature modulation only after it has reached the sample surface due to the superposition of thermal waves moving back to the surface [25]. Consequently, the mean pathlength of the photopyroelectric thermal wave is larger than that of gas-phase PAS and the P^2E phase spectra are expected to contain deep-bulk information not accessible to the PA phase spectrum [4].

The PC phase spectrum is independent of the photocarrier density, which is temporally constant and varies with photon energy. It depends, however, on the carrier diffusion length [26]

$$L_n(\omega)=\frac{L_n}{(1+i\omega\tau)^{1/2}}, \tag{4}$$

where τ is the photocarrier lifetime and L_n is the diffusion length under dc field conditions. In the limit $\omega\tau \ll 1$, the PC phase is expected to be independent of the mechanism producing the photocurrent. Thus, at low modulation frequencies

$$f \ll 1/2\pi\tau \tag{5}$$

a spectrally flat PC phase response would be expected, in agreement with Fig. 9b. The large standard deviations at $\lambda<510$ nm are due to the extremely low PC signals at that region, Fig. 9a.

3. Conclusions

The present work has established the use of P^2ES as a spectroscopic technique sensitive to the non-radiative energetics of electronic defect centers in the sub-band-gap region of defect-rich semiconductors such as n-CdS single crystal. The spectral domination of the sub-band-gap region by defect-related heat release was shown to be complete, leading to spectral feature inversions between the intact and the defective CdS crystals. This behavior shows that P^2E spectra are much more sensitive to defect centers than similar PA spectra [5], where both interband transition and defect-related spectral peaks of similar magnitudes were found to co-exist. The high non-radiative defect center sensitivity of P^2ES, coupled with the extreme

simplicity of the experimental system may possibly establish this technique as the leading candidate for spectroscopic studies of defect physics in crystalline and non-crystalline semiconductors.

Acknowledgements. The authors wish to acknowledge the financial support of the Natural Sciences and Engineering Research Council of Canada (NSERC) throughout the duration of this work. One of us (A.M.) is also grateful to Dr. H. Coufal for supplying the Inficon housing for the experiments, and to one of the referees for valuable comments and suggestions.

References

1. A.N. Georgobiani: Soviet Phys.-Usp. (Engl. Transl.) **17**, 424–437 (1974)
2. J.J. Song, W.C. Wang: J. Appl. Phys. **55**, 660–664 (1984)
3. K. Wasa, K. Tsubouchi, N. Mikoshiba: Jpn. J. Appl. Phys. **19**, L475–L478 (1980)
4. A. Mandelis, E.K.M. Siu: Phys. Rev. B **34**, 7209–7221 (1986)
5. T. Dioszeghy, A. Mandelis: J. Phys. Chem. Solids **47**, 1115–1128 (1986)
6. E.K.M. Siu, A. Mandelis: Phys. Rev. B **34**, 7222–7232 (1986)
7. A. Mandelis: In *Photoacoustic and Thermal Wave Phenomena in Semiconductors*, ed. by A. Mandelis (Elsevier, New York 1987) (in press)
8. H. Coufal: Appl. Phys. Lett. **44**, 59–61 (1984)
9. A. Mandelis: Chem. Phys. Lett. **108**, 388–392 (1984)
10. D. Dadarlat, M. Chirtoc, R.M. Candea, I. Bratu: Infrared Phys. **24**, 469–471 (1984)
11. H. Coufal: Appl. Phys. Lett. **45**, 516–518 (1984)
12. A. Mandelis, M.M. Zver: J. Appl. Phys. **57**, 4421–4430 (1985)
13. H. Coufal, A. Mandelis: In *Photoacoustic and Thermal Wave Phenomena in Semiconductors*, ed. by A. Mandelis (Elsevier, New York 1987) (in press)
14. Data concerning PVDF KYNAR™ pyroelectric film can be found in "KYNAR™ Piezo Film Technical Manual", Pennwalt Corp. (1983); Information on PVDF can be found in: Ferroelectrics **32** (1981)
15. K. Tanaka, K. Sindoh, A. Odajima: Rep. Progr. Polym. Phys. Jpn. (in press)
16. T. Hata, T. Hatsuda, M. Kawakami, Y. Sato: Jpn. J. Appl. Phys. **24**, Suppl. **24-1**, 204–206 (1985)
17. H. Coufal, S. Peterson: IBM Tech. Discl. Bull. **27**, 5538 (1985)
    H. Coufal: Private communication
18. C.L. Cesar, H. Vargas, J. Mendes Filha, L.C.M. Miranda: Appl. Phys. Lett. **43**, 555–557 (1983)
19. A.C. Tam, H. Coufal: Appl. Phys. Lett. **42**, 33–35 (1983)
20. R. Takaue, M. Matsunaga, K. Hosokawa: J. Appl. Phys. **56**, 1543–1545 (1984)
21. P. Rochon, T.J. Racey: J. Photoacoust. **1**, 475–484 (1983–1984)
22. I.N. Bandeira, H. Closs, C.C. Ghizoni: J. Photoacoust. **1**, 275–290 (1982)
23. T. Hata, Y. Sato, M. Kurebayashi: Jpn. J. Appl. Phys. **22**, Suppl. **22-3**, 205–207 (1983)
24. A. Mandelis, Y.C. Teng, B.S.H. Royce: J. Appl. Phys. **50**, 7138–7146 (1979)
25. G. Busse, A. Rosencwaig: J. Photoacoust. **1**, 365–369 (1982–1983)
26. J.P. McKelvey: *Solid State and Semiconductor Physics* (Harper & Row, New York 1966) Sect. 13.6